# Whole heart detailed and quantitative anatomy, myofibre structure and vasculature from X-ray phase-contrast synchrotron radiation-based micro-CT

Anna Gonzalez-Tendero PhD[1], Chong Zhang PhD[2,3], Vedrana Balicevic[4], Rubén Cárdenes PhD[1,2], Sven Loncaric PhD[4], Constantine Butakoff PhD[2], Bruno Paun[2], Anne Bonnin PhD[5,6], Patricia Garcia-Cañadilla PhD[2], Emma Muñoz-Moreno PhD[1], Eduard Gratacós PhD[1], Fatima Crispi PhD[1], Bart Bijnens PhD[2,7]

*[1] Fetal i+D Fetal Medicine Research Center, BCNatal – Barcelona Center for Maternal-Fetal and Neonatal Medicine (Hospital Clínic and Hospital Sant Joan de Deu), IDIBAPS, University of Barcelona, and Centre for Biomedical Research on Rare Diseases (CIBER-ER), Barcelona, Spain;*
*[2]PhySense, DTIC, Universitat Pompeu Fabra, Barcelona, Spain;*
*[3]CellNetworks, Heidelberg, Germany*
*[4]Faculty of Electrical Engineering and Computing, University of Zagreb, Zagreb, Croatia;*
*[5]European Synchrotron Radiation Facility, Grenoble, France*
*[6]Paul Scherrer Institut, Villigen, Switzerland*
*[7]ICREA, Barcelona, Spain*

Adress for correspondence:

Prof. Bart Bijnens
Universitat Pompeu Fabra - DTIC
Carrer de Tànger, 122-140
ES–08018 Barcelona (Spain)
Tel. +34 61 501 6853
e-mail: bart.bijnens@upf.edu

**Short title:** Synchrotron imaging for assessing myocardium

**Word count:** 5024

**Journal subject codes:** [115] remodelling; [124] Cardiovascular imaging agents/Techniques; [130] Animal models of human disease; [87] Coronary circulation; [150] Imaging; [104] Structure.

## ABSTRACT

**Background:** While individual cardiac myocytes only have a limited ability to shorten, the heart efficiently pumps a large volume-fraction thanks to a cell organization in a complex 3D fibre structure. Subclinical subtle cardiac structural remodelling is often present before symptoms arise. Understanding and early detection of these subtle changes is crucial for diagnosis and prevention. Additionally, personalized computational modelling requires knowledge on the multi-scale structure of the whole heart and vessels.

**Methods and results:** We developed a rapid acquisition together with visualization and quantification methods of the integrated microstructure of whole in-vitro rodents hearts using synchrotron based X-ray phase-contrast tomography. These images are formed not only by X-ray absorption by the tissue, but also by wave propagation phenomena, enhancing structural information, thus allowing to raise tissue contrast to an unprecedented level. We used a (ex-vivo) normal rat heart and fetal rabbit hearts suffering intrauterine growth restriction as a model of subclinical cardiac remodelling to illustrate the strengths and potential of the technique. For comparison, histology and diffusion tensor magnetic resonance imaging was performed.

**Conclusions:** We have developed a novel, high resolution, image acquisition and quantification approach to study a whole in-vitro heart at myofibre resolution, providing integrated 3D structural information at microscopic level without any need of tissue slicing and processing. This superior imaging approach opens up new possibilities for a systems approach towards analysing cardiac structure and function, providing rapid acquisition of quantitative microstructure of the heart in a near native state.



**Key words**: myocardial remodelling; myofibre structure; coronary vasculature; synchrotron phase-contrast CT.

## INTRODUCTION

For structural/functional (image-based) quantification, cardiac chambers are often simplified to ellipsoid-like volumes. In reality, macroscopic shape is variable and complex trabeculations and intra-cavitary structures, such as papillary muscles and tendinous chordea, as well as false tendons, are present. At microscopic level, myocardium is made of millions of myocytes aggregated as a 3D mesh within a supporting fibrous matrix.[1] Additionally, a coronary tree, starting from epicardial arteries, branching into a complex network, penetrates the wall.

Myocytes are aggregated and aligned in a predominant direction (fibres) within the wall.[1] At the epicardium as well as endocardium, myocytes are tangential to the epicardium and oblique to the long-axis, with a predominant longitudinal (base-apex) direction, while in mid-myocardium predominantly circumferential. The change in angle is gradual. Ejection results from complex 3D movement that involves longitudinal contraction, circumferential contraction as well as rotation/twisting.[2]

While (genetic) cardiomyopathies or fibrosis will significantly change local microstructure, more subclinical conditions may lead only to subtle changes. An example is intrauterine growth restriction (IUGR) where fetal hypoxia and volume/pressure overload induce functional remodeling and change cardiac shape to be more globular in IUGR[3]. The 3D cardiac architecture is established early in prenatal life and fibre orientation is sensitive to changes in mechanical load and hypoxia.[4] Additionally, IUGR induces adaptive changes to coronaries which responds to conditions of chronic hypoxemia by a substantial increase in cross-sectional area[5].

Therefore, to understand disease progression, integrating information about individual cells and their spatial organization is essential. Additionally, contemporary computational modelling requires detailed whole heart 3D morphology at a resolution including all relevant details. Several approaches have been used, both through direct visualization (microscopy or micro-magnetic resonance imaging (MRI)/computed tomography (CT)) or through inference by

assessing local tissue properties (diffusion tensor MRI (DTMRI) or echocardiography). However, detecting orientation of individual myocytes, especially in the whole heart, is still a major challenge[6]. Histology/microscopy provides sufficient detail, but hardly allows imaging whole hearts, and artefact-prone slicing/processing is required.[7] High resolution/field MRI (including DTMRI)[8] still has a suboptimal spatial resolution (~50 µm) and scan times are extremely long. Classical, absorption-based, micro-CT, after iodine staining, shows promise,[9,10] but organ preparation is challenging and extracting integrated microstructure, including myofibres and vessels is hardly feasible.

In this study we propose an integrated, high resolution, image acquisition and quantification approach to study whole hearts at myofibre (µm-) resolution, providing structural information at microscopic level without the need of slice-processing and illustrate how this can be used to assess subclinical remodelling. Imaging is based on X-ray phase-contrast imaging (X-PCI), which has emerged as an alternative X-ray-based approach providing enhanced contrast in some biological tissues[11] and is recently showing potential for clinical applications and to improve the diagnostic work-up.[12]

## MATERIAL AND METHODS

New Zealand white rabbits and Wistar rats were provided by a certified breeder. Animal handling/procedures were performed in accordance to regulations and with approval of the local Ethics Committee (permit numbers: 313/11 with date of approval 19/07/2011 for rabbits, and 110/13, 505/13 with date of approval 18/07/2013 for rats).

A rat (25 days) was anesthetized with isofluorane 3% and oxygen 2 ml/min. Heparin 500U was administered as well as saturated potassium chloride to arrest the heart. After thoracotomy, a phosphate-buffer saline solution was used to rinse and 10% formalin to fix the heart, which was excised and immersed in formalin.

A validated IUGR rabbit model was reproduced.[13] Briefly, at 25 days gestation both uterine horns were exteriorized and one selected as IUGR, in which selective ligature of 40-50% of utero-placental vessels of each gestational sac was performed. The abdomen was closed and animals were kept in regular conditions and fed a diet of standard chow and water *ad libitum.* At 30 days gestation, a caesarean was performed. After anaesthesia with intramuscular ketamine and xylazine, the fetal chest was opened and hearts were prepared as above. Before imaging, hearts were dehydrated with ethanol and, to avoid motion artefacts, immobilized in 1% agarose. For the DTMRI, the heart of the mother, was arrested and processed using the same approach as the rats.

### Data acquisition

### X-ray Phase Contrast Imaging

3D datasets of the whole heart have been obtained at the European Synchrotron Radiation Facility (ESRF - ID19 beamline[14], Grenoble, France) with propagation-based phase-contrast tomography.[12] X-PCI is a technique used to increase the image contrast, and thus the sensitivity of discriminating different materials. This improves imaging of soft materials or materials which have a similar density. Several approaches have been suggested to perform

X-PCI, either using synchrotron radiation from more conventional X-ray sources[12] and by either or not adding additional optical components (e.g. interferometers or two-crystal diffractometers). For example, X-PCI using Talbot interferometers has been used in different cardiovascular pathologies[15,16]. Propagation-based X-PCI is a fast and high resolution approach that requires no additional optical components and was therefore chosen for the acquisition. In this approach, by increasing the distance between the sample and the detector to record the radiography, the phase jumps that occur at the edges of two different materials (i.e. two different index of refraction) will be enhanced. Using a phase retrieval approach, the local phase shift is retrieved and is directly proportional to the density.

The current experiments were done using a 19 keV parallel X-ray beam and the sample was localized at about 145m from the source. The distance between the sample and the detector (FReLON CCD, i.e. fast readout low noise charged-coupled device, camera - ESRF Instrument Support Group, Grenoble, France) was tuned to 1100mm to get an optimal propagation distance to visualise the cardiac microstructure.

The field of view was 5.68x15.96mm, with isotropic pixels of 7.43µm. The sample was at room temperature and placed on a holder. After positioning it at the stage's centre of rotation, it was rotated over 360º acquiring 2499 projections (exposure time 0.3s per projection). Total acquisition time for each position was 14min. Four to five sequential acquisitions (overlap 363 slices - 2,697mm) always from base to apex, were necessary to cover the whole heart along its long axis. Additionally, in order to apply the usual flat-field correction, 41 flat images and 21 dark images have been acquired. Flat images remove mainly artefacts caused by the beam illumination non-uniformity and dark images allow to correct from the electronic noise of the CCD camera. The flat-field correction is applied before the reconstruction procedure, by a pixel-by-pixel computation i.e. (Radiography-Dark)/(Flat-Dark). Therefore, total acquisition time was approximately 1-1.25 hours/sample (4-5 chunks).

Each projection series was reconstructed using filtered back-projection[17]. Reconstructed volumes were converted to 16-bit tiff images and merged into a single dataset. In all cases, the whole heart was in the resulting 3D dataset. An example of an unprocessed dataset will be made available for download.

Images were analysed with Fiji (reslicing/rendering and vessel quantification),[18] ICY (rendering)[19] and ilastik (vessel segmentation)[20] and in-house developed Matlab (The MathWorks,Natick, MA,USA) software for fibre analysis.[21] The analysis and processing of the different data sets were performed by different people including biologists, clinicians, physicists and biomedical engineers. The image analysis was performed without any information beforehand. The correspondence of the regions with morphology was performed by the clinicians and biologists who have an extensive knowledge of cardiac anatomy.

**MRI DTI**

MRI acquisition was conducted on a 7.0 T Bruker BioSpec 70/30 horizontal animal scanner (BrukerBioSpin, Ettlingen, Germany). Ex-vivo imaging was performed on an excised adult rabbit heart that had been fixed in formalin and stored in phosphate-buffered saline (PBS). Imaging an adult heart was chosen for practicalities and difficulties to scan a fetal heart. Diffusion-weighted images (DWI) were acquired using a standard diffusion sequence including 126 diffusion directions with a b-value of 3000 s/mm$^2$ and a baseline image without diffusion (b=0 s/mm$^2$). Other acquisition parameters were Echo Time (TE)=26ms, Repetition Time (TR)=250 ms, Field of View (FOV)=36.4x26.6x49.0 mm$^3$ and spatial resolution 0.7x0.7x0.7 mm$^3$. The total scan time was 11 hours and 38 minutes.

**Histology**

Formalin-fixed fetal hearts were dehydrated, embedded in paraffin and 10µm slices were obtained in a microtome. After deparaffination, slices were stained with conventional hematoxylin and eosin staining. Images were acquired with a camera (Leica DFC425 C, Leica Microsystems GmbH, Heerbrugg, Switzerland) coupled to an optical microscope (Leica DM

1000, Leica Microsystems GmbH, Wetzlar, Germany) at 20x magnification. A total of 272 overlapping images with a minimum of 50% of overlapping and a resolution of 2592x1944 pixels (571 x 429 µm) were acquired from the whole heart and stitched using Image Composite Editor (ICE, Microsoft Research, Redmond, WA) software.

**Coronary segmentation**

Coronaries cover only a small part of the large volumetric datasets (~0.5%), and are best distinguished by a boundary that may be incomplete. The image analysis software *ilastik*,[20] offers a seeded segmentation module, *Carving*, which provides semi-automated segmentation based on sparse user scribbles.[22] For each object of interest, i.e. vascular tree, it requires "inside" and "outside" seeds as input to propagate to explain the entire volume, using a biased watershed algorithm[22]. Several iterations maybe needed to achieve segmentation. This workflow also provides the uncertainty estimation of the current segmentation, thus guiding the user to locations where additional input may be helpful.

The vessel local lumen diameter is approximated as the diameter of the largest fitting sphere (Fiji Local Thickness plugin[23]).

**Fibre-orientation quantification**

**X-ray phase-contrast imaging (X-PCI)**

For calculating the myocardial fibre-orientation, the gradient structure-tensor method was used. While in DTMRI, spatial anisotropy of diffusion is assessed,[24] the structure-tensor calculates the structural anisotropy from the image appearance, thus assessing local dominant directions (i.e. fibres).[21]

For each voxel, oriented gradient magnitudes in x, y and z-directions were obtained using central difference. The local structure-tensor within a 3D neighbourhood is then defined as:

$$\mathrm{ST} = \begin{bmatrix} \sum g_x^2 & \sum g_x g_y & \sum g_x g_z \\ \sum g_y g_x & \sum g_y^2 & \sum g_x g_z \\ \sum g_z g_x & \sum g_z g_y & \sum g_z^2 \end{bmatrix} \quad \text{[Eq1]}$$

where $g_x$ denotes the gradient in the x-axis etc., and $\Sigma$ denotes integration of selected oriented gradients in the neighbourhood defined as a cube surrounding the voxel. Eigen-decomposition of ST transforms the given gradient space into a space defined with three orthogonal vectors encoding the appearance of a tubular structure, i.e. fibre. The smallest eigenvalue corresponds to the vector pointing in the fibre direction (since it is associated to minimal image intensity variation). To calculate fibre angle maps, we transform these vectors from Cartesian to a cylindrical coordinate system, where the axis corresponds to the left ventricular (LV) long axis. For the smallest eigenvalue vector, the inclination angle was then calculated as an angle between the transverse plane and the vector projection to the local tangent plane.

**MRI DTI**

A median Otsu threshold[25] was computed on the baseline image to obtain a mask of the cardiac tissue to segment it from the background. The mask was applied to all the DWI. Diffusion tensor image (DTI) was estimated in the masked volume and streamlines assessed by a deterministic tractography algorithm considering a threshold of fractional anisotropy of 0.2, using Dipy.[26] From the DTI, eigenvalues and eigenvectors of the diffusion tensor were computed, and the main eigenvector, describing the main fiber direction, was considered to obtain the helix angle, computed as $\pi/2 - \cos^{-1}(\vec{e}_1 \cdot \vec{l}_{axis})$ , where $\vec{l}_{axis}$ is the unitary vector in the direction of the long axis of the left ventricle and $\vec{e}_1$, the main eigenvector of the tensor matrix.

## RESULTS

All reconstructed datasets covered the whole heart and provided 3D detail that has not been generated for a whole heart at this resolution before. One rat, one normal fetal rabbit and one IUGR fetal rabbit heart were processed.

Figure 1 shows the images obtained from the rat heart. Figure 1 (A-C) shows the originally reconstructed short axis slices at aortic valve (1A) and mid-ventricular level (1B), as well as a longitudinal reslice through aortic valve and apex (1C). Cardiac substructures can be clearly differentiated (atria, ventricles, great vessels and valves). Intramural vessels as well as local fibre directions can be recognized (1B). When visualizing data using volume-rendering (Figure 1D-G), the detailed architecture of tricuspid valve apparatus (1D) and aortic valve (1E) can be clearly visualized. Additionally, details of local wall complexity (such as atrial pectinate muscles - 1F/G) and part of the vasculature are visible.

Figure 2 shows a detailed view of the aortic wall (2A) as well as from the right ventricular (RV) free wall (2B) and LV lateral wall (2C) from the same rat heart. In the aortic wall, spiral-like structures can be distinguished, corresponding to elastin providing support and elasticity. In the ventricular walls, besides clearly visible vessels, predominant directions of fibres can be observed. Longitudinally oriented cell-aggregates show as dot-like structures in short-axis, while circumferential fibres are line-like. From this, it can be seen that in the LV, in epicardial, as well as endocardial sides, fibres are predominantly longitudinal while in mid-wall, they are more circumferential. However, in the RV, fibres at endocardial sides are mainly longitudinal while mostly circumferential at epicardial sides. The structures seen in this type of images have been shown to correspond well to histology[27]. Video 1 shows the (edge-enhanced) whole rat heart dataset from short-axis slices. The intramural course of coronary vessels is easily traceable and the oblique course of fibres gives the impression of flow within the myocardium with different direction at both edges of the walls. The spiral like arrangement towards the apex is clearly shown.

Figure 3 shows surface rendered images of cuts through the fetal rabbit hearts. The IUGR heart (C,D) is clearly smaller than the normal (A,B). Additionally, coronaries are clearly dilated and much more prominent in IUGR. In the RV cut (B,D), both chordal as well as false tendons

can be depicted. Video 2 shows cuts through the whole heart, showing all endo- and epicardial structures as well as the vasculature.

Figure 4 (and video 3) shows the segmented arterial trees for both fetal rabbit hearts (A,C) as well as a colour-visualization of estimated local lumen diameter (B,D) where coronary dilatation in IUGR (C,D) can be clearly observed. In Figure 4 (E), the normalized histogram of lumen diameter shows that coronary size in IUGR is shifted to the right (i.e. larger diameter) of the histogram, and the relative amount of vessels with smaller diameters (left side) in normal hearts is higher.

Figure 5 shows local helix angles within a slice (mid ventricular) of control (A) and IUGR (B) hearts, together with a visualization of the resulting 3D fibre structure in IUGR (C: fibre angles within one plane; D: 3D fibre tracking throughout the wall). The gradual change from predominantly longitudinal at endocardial side, towards more circumferential in mid-myocardium and again longitudinal at epicardial can be observed. A rather abrupt change in mid-septum is present as was suggested earlier.[28] The bottom plots show the histogram of the distribution of the angles within the LV (E) and RV wall (F) (IUGR). From this distribution, as well as from the slice showing the regional angles, it can be observed that in the LV, fibres are predominantly longitudinal with both positive and negative angles, corresponding to epi- and endocardial regions. However, in the RV, endocardium is clearly predominantly longitudinal, but epicardium is not, resulting in an imbalance of positive and negative large angles in the distribution.

Figure 6 (A) shows local helix angles within a slice (mid ventricular) together with a visualization of the resulting 3D fibre structure (B) of a control adult rabbit heart determined by MRI DTI analysis. The low resolution of MRI DTI images, demonstrated by the low number of voxels across the lateral walls, clearly shows the gradual change in the local angle from endo- to epicardium but makes it very difficult to quantify this in detail, especially in the more complex regions such as the inflow/outflow tracks or RV/LV junction. Despite this, it can be

seen again how fibers are more circumferential in mid-myocardium while in the endo and epicardium are more longitudinal, in agreement with what is estimated from X-PCI images.

Figure 7 (A) shows the optical image of a whole organ histological section of the control fetal rabbit heart similar to the X-PCI section (B) to illustrate the structural similarity between them. The bundle of myocytes (in red) surrounded by the extracellular matrix (white) are distinguish in the histological section (A,C). Capillaries with red blood cells are also clearly visible. The bottom images show a zoomed-in area of the LV lateral wall (C,D). Even though the difficulty of clearly determine the angles of fiber-like arrangement of myocytes in the histological section due to the immature state of the sample, the same gradual change in the directionality of the fibers observed in X-PCI images (D), is also visible. Remark that the fetal myocardium, where myocytes (-junctions) are not fully developed yet, are much more difficult to image/analyse compared to fully mature myocardium where fibre-orientation is much more clear. Still, the X-PCI images provide enough structural detail to extract local tissue orientations.

## DISCUSSION

We described a comprehensive, integrated approach for non-destructive acquisition, visualization and quantification of (sub-) structure of whole in-vitro rodent hearts at almost cell-level resolution.

This approach allows rapid whole heart imaging to quantify morphological remodelling of all substructures within different cardiac components. Both myocardial tissue and vessels can be extracted and interrelated from the same dataset, with the ability to extract local orientation of myocytes (=fibres) and relate it to location within wall and surrounding vasculature. Additionally, global chamber geometry, including detailed visualization of trabeculations and (false) tendons is provided.

These datasets provide a unique source of information where tissue properties can be quantified/compared within the 3D structure for purposes of describing changes induced by genetic/acquired disease, even if remodelling is subtle and not detectable by current imaging modalities.

The data richness, together with resolution and image contrast, allows use of state-of-the-art analysis tools to quantify and visualize different substructure of the whole 3D dataset. To extract coronaries, we employed an interactive segmentation using sparse user-specified seeds. The ability to discriminate local predominant direction of myocyte-aggregates allows for quantification of transmural fibre distribution by extracting 3D components of the local structure-tensor using gradient calculations together with fibre-tracking approaches similar to those used in DTMRI. This allows optimal re-use of the vast spectrum of analysis tools, while offering the possibility to combine approaches from high-resolution data with techniques developed for lower resolution (clinical) modalities.

Additionally, both superior resolution as well as the fact that all substructures can be recognized and segmented while originating from single dataset, enable to obtain structural

data required for performing computational modelling of the heart as a functional organ. Current approaches often get image-based overall geometry, but have to incorporate fibre structure from low-resolution (ex-vivo) DTMRI or statistical models developed from microscopy.[29] This offers a wealth of new possibilities to improve models, especially towards more individual simulations and comparing control and pathological specimens.

The proposed imaging is based on X-PCI tomography, which is available in contemporary synchrotron facilities. It is currently the only non-destructive method that provides the resolution needed to resolve details of the size of individual myocytes (<10 µm). Even if some microCTs can provide the resolution, X-ray absorption imaging does not provide contrast needed to discriminate microstructural details within cardiac tissue. Vessels and fibres can only be detected when a contrast agent is used. However, this is highly artefact prone since a homogeneous contrast distribution along myofibres and within vasculature is very challenging.

With X-PCI, not only local X-ray absorption is quantified, but it additionally captures wave-propagation phenomena that enhances subtle differences in tissues and improves tissue/vessel contrast and thus helps capturing details on local predominant myofibre direction.[27] Therefore, X-PCI is far superior to (contrast-enhanced) X-ray absorption when studying cardiac microstructure. While a lot of research is going on to allow for X-PCI based on traditional CTs,[30] and compact light sources are under development[31,32] currently, high-resolution X-PCI is mainly available in synchrotrons. It is an expanding field in synchrotrons and has shown great promise for non-destructive visualization/quantification of samples from different origins and application fields (paleontology, biology, material-science). Extending the use of these large-infrastructure research facilities, funded by (inter-)national research organization, towards cardiac applications, opens up new possibilities for studying cardiovascular development, pathophysiological remodelling and therapeutic targets.

To illustrate the potential of the approach, besides a healthy rat, we also scanned a control and IUGR fetal rabbit heart. The resolution and absence of complicated preparation and

imaging, allowed studying the micro-architecture of the fetal heart, which is challenging otherwise. Additionally, we have shown that integrated assessment of organ morphology, vasculature and fibre-structure provides a way to quantify subtle (sub-clinical) remodelling induced *in utero*, beyond gross changes induced by genetic alterations. We observed that, while the heart is smaller, coronaries are clearly dilated, most probably as adaptation to haemodynamic challenges induced by hypoxia/hyponutricia. Additionally, the gradual change of fibre-direction can be quantified.

In this report, we describe preliminary results of in-vitro rodent hearts, mainly focusing on direct visualization and quantification of remodelling induced by IUGR which has been demonstrated to induce a remodelling at the organ level,[33,3] as well as at the cellular and subcellular level[34]. However the precise mechanisms leading to increased risk of cardiovascular disease in adulthood are still not well understood.

## LIMITATIONS

While X-PCI is highly promising for quantification of the integrated multi-scale cardiac structure and its components, currently it is limited to synchrotron-facilities and therefore not easily accessible. Current synchrotrons have limited fields-of-view. Depending on the facility, the current field of view is in the order of 10-15 mm for one-shot imaging. Also, an improved resolution (pixels sizes <1$\mu$m) can be achieved, but this results in an even smaller field of view. Using stitching approaches, larger samples, or small samples at higher resolution, can be scanned but this is making it much more time-consuming. Therefore, larger hearts than rodents are currently challenging.

On-going research in CT-technology (both microCT and clinical scanners), compact sources and detectors might lead to more widespread access and.

In our study, we examined in-vitro rodent hearts. However, while challenging, the technology should be applicable in-vivo. In fact, X-PCI has been used to perform mammographic in-vivo imaging allowing greater precision in the assessment of breast cancer[35].

## CLINICAL PERSPECTIVES

While the current setup, using synchrotron facilities, makes human applications limited, the progress in the field of X-PCI technology as well as reconstruction approaches (a.o. efficient stitching) can lead to more widespread availability. In this paper we show that X-PCI can assess the detailed macro-anatomy as well as obtain information from the micro-structure. When used with post-mortem tissue, this imaging approach could be used for non-destructive detailed 3D tissue-characterisation, thus overcoming some of the current limitations of traditional histology. For example, fast and non-destructive post-mortem diagnosis of fetuses could be achieved at higher resolution/contrast compared to other modalities; 3D detailed imaging of endo-myocardial biopsies could provide improved diagnostic yields. Additionally, if X-PCI becomes available in clinical scanners, in-vivo assessment of tissue structure, fibrosis, vessels might be achievable and would not require the use of contrast agents.

## CONCLUSION

In conclusion, we have developed a novel, high resolution, non-destructive approach towards visualizing and quantifying the microstructure of whole hearts at myofibre resolution, providing structural information at microscopic level without need of slice processing. This opens up new possibilities for a systems-medicine approach towards remodelling, providing fast acquisition of hearts in a near native state without processing artefacts. Studying fetal and rodent hearts is particularly challenging due to their size and the proposed approach could help to understand normal organ development and remodelling in disease from earliest stages of life.


## ACKNOWLEDGMENTS

We acknowledge ESRF for provision of synchrotron-radiation facilities.

## FUNDING SOURCES

This study was partly supported by Ministerio de Economia y Competitividad (SAF2012-37196;TIN2014-52923-R); Instituto de Salud Carlos III (PI11/00051, PI11/01709, PI12/00801, PI14/00226) integrados en el Plan Nacional de I+D+I y cofinanciados por el ISCIII-Subdirección General de Evaluación y el Fondo Europeo de Desarrollo Regional (FEDER) “Otra manera de hacer Europa”;the EU-FP7 for research, technological development and demonstration under grant agreement VP2HF (no611823); The Cerebra Foundation for the Brain Injured Child (Carmarthen, UK);Obra Social “la Caixa” (Barcelona, Spain); Fundació Mutua Madrileña and Fundació Agrupació Mutua (Spain).

## REFERENCES


1. Anderson RH, Ho SY, Redmann K, Sanchez-Quintana D, Lunkenheimer PP. The anatomical arrangement of the myocardial cells making up the ventricular mass. *Eur J Cardiothorac Surg* 2005;**28**:517–525.

2. Bijnens B, Cikes M, Butakoff C, Sitges M, Crispi F. Myocardial motion and deformation: What does it tell us and how does it relate to function? *Fetal Diagn Ther* 2012;**32**:5–16.

3. Crispi F, Bijnens B, Figueras F, Bartrons J, Eixarch E, Noble F Le, et al. Fetal growth restriction results in remodeled and less efficient hearts in children. *Circulation* 2010;**121**:2427–2436.

4. Tobita K, Garrison JB, Liu LJ, Tinney JP, Keller BB. Three-dimensional myofiber architecture of the embryonic left ventricle during normal development and altered mechanical loads. *Anat Rec A Discov Mol Cell Evol Biol* 2005;**283**:193–201.

5. Thornburg KL, Reller MD. Coronary flow regulation in the fetal sheep. *Am J Physiol* 1999;**277**:R1249-60.

6. Mekkaoui C, Porayette P, Jackowski MP, Kostis WJ, Dai G, Sanders S, et al. Diffusion MRI tractography of the developing human fetal heart. Bauer WR, ed. *PLoS One* Public Library of Science; 2013;**8**:e72795.

7. Jouk P-S, Mourad A, Milisic V, Michalowicz G, Raoult A, Caillerie D, et al. Analysis of the fiber architecture of the heart by quantitative polarized light microscopy. Accuracy, limitations and contribution to the study of the fiber architecture of the ventricles during fetal and neonatal life. *Eur J Cardiothorac Surg* 2007;**31**:915–921.

8. Teh I, McClymont D, Burton RAB, Maguire ML, Whittington HJ, Lygate CA, et al. Resolving fine cardiac structures in rats with high-resolution diffusion tensor imaging. *Sci Rep* 2016;**6**:30573.

9. Aslanidi O V, Nikolaidou T, Zhao J, Smaill BH, Gilbert SH, Holden A V, et al. Application of micro-computed tomography with iodine staining to cardiac imaging, segmentation, and computational model development. *IEEE Trans Med Imaging* 2013;**32**:8–17.

10. Stephenson RS, Boyett MR, Hart G, Nikolaidou T, Cai X, Corno AF, et al. Contrast enhanced micro-computed tomography resolves the 3-dimensional morphology of the cardiac conduction system in mammalian hearts. Roeder RK, ed. *PLoS One* Public

Library of Science; 2012;**7**:e35299.

11. Cloetens P, Barrett R, Baruchel J, Guigay J-P, Schlenker M, N SD and CH, et al. Phase objects in synchrotron radiation hard x-ray imaging. *J Phys D Appl Phys* IOP Publishing; 1996;**29**:133–146.

12. Bravin A, Coan P, Suortti P. X-ray phase-contrast imaging: from pre-clinical applications towards clinics. *Phys Med Biol* 2013;**58**:R1-35.

13. Eixarch E, Figueras F, Hernandez-Andrade E, Crispi F, Nadal A, Torre I, et al. An experimental model of fetal growth restriction based on selective ligature of uteroplacental vessels in the pregnant rabbit. *Fetal Diagn Ther* 2009;**26**:203–211.

14. http://www.esrf.eu/UsersAndScience/Experiments/Imaging/ID19/BeamlineDescription/GeneralDescription.

15. Zanette I, Bech M, Rack A, Duc G Le, Tafforeau P, David C, et al. Trimodal low-dose X-ray tomography. *Proc Natl Acad Sci* National Acad Sciences; 2012;**109**:10199–10204.

16. Tsukube T, Yagi N, Hoshino M, Nakashima Y, Nakagawa K, Okita Y. Impact of synchrotron radiation-based X-ray phase-contrast tomography on understanding various cardiovascular surgical pathologies. *Gen Thorac Cardiovasc Surg* 2015;**63**:590–592.

17. Mirone A, Brun E, Gouillart E, Tafforeau P, Kieffer J. The PyHST2 hybrid distributed code for high speed tomographic reconstruction with iterative reconstruction and a priori knowledge capabilities. *Nucl Instruments Methods Phys Res Sect B Beam Interact with Mater Atoms* 2014;**324**:41–48.

18. Schindelin J, Arganda-Carreras I, Frise E, Kaynig V, Longair M, Pietzsch T, et al. Fiji: an open-source platform for biological-image analysis. *Nat Methods* 2012;**9**:676–682.

19. Chaumont F de, Dallongeville S, Chenouard N, Hervé N, Pop S, Provoost T, et al. Icy: an open bioimage informatics platform for extended reproducible research. *Nat Methods* 2012;**9**:690–696.

20. Sommer C, Sträehle C, Köthe U, Hamprecht FA. Ilastik: Interactive learning and segmentation toolkit. *Proceedings - International Symposium on Biomedical Imaging* IEEE; 2011. p. 230–233.

21. Baličević V, Lončarić S, Cárdenes R, Gonzalez-Tendero A, Paun B, Crispi F, et al. Assessment of myofiber orientation in high resolution phase-contrast CT images. *Functional Imaging and Modeling of the Heart* Springer International Publishing; 2015. p. 111–119.

22. Sträehle CN, Köthe U, Knott G, Hamprecht FA. Carving: scalable interactive segmentation of neural volume electron microscopy images. *Med Image Comput Comput Assist Interv* 2011;**14**:653–660.

23. Hildebrand T, Ruegsegger P. A new method for the model-independent assessment of thickness in three-dimensional images. *J Microsc* Blackwell Science Ltd; 1997;**185**:67–75.

24. Scollan DF, Holmes A, Zhang J, Winslow RL. Reconstruction of cardiac ventricular geometry and fiber orientation using magnetic resonance imaging. *Ann Biomed Eng* 2000;**28**:934–944.

25. Otsu N. A threshold selection method from gray-level histograms. *IEEE Trans Syst Man Cybern* IEEE; 1979;**9**:62–66.

26. Garyfallidis E, Brett M, Amirbekian B, Rokem A, Walt S van der, Descoteaux M, et al. Dipy, a library for the analysis of diffusion MRI data. *Front Neuroinform* 2014;**8**:8.

27. Mirea I, Varray F, Zhu YM, Fanton L, Langer M, Jouk PS, et al. Very high-resolution imaging of post-mortem human cardiac tissue using X-ray phase contrast tomography. *Functional Imaging and Modeling of the Heart* Springer International Publishing; 2015. p. 172–179.

28. Boettler P, Claus P, Herbots L, McLaughlin M, D'hooge J, Bijnens B, et al. New aspects of the ventricular septum and its function: an echocardiographic study. *Heart* 2005;**91**:1343–1348.

29. Romero D, Sebastian R, Bijnens BH, Zimmerman V, Boyle PM, Vigmond EJ, et al. Effects of the purkinje system and cardiac geometry on biventricular pacing: a model study. *Ann Biomed Eng* 2010;**38**:1388–1398.

30. Hetterich H, Willner M, Fill S, Herzen J, Bamberg F, Hipp A, et al. Phase-contrast CT: qualitative and quantitative evaluation of atherosclerotic carotid artery plaque. *Radiology* 2014;**271**:870–878.

31. Carroll FE. Tunable monochromatic X rays: a new paradigm in medicine. *AJR Am J*

*Roentgenol* 2002;**179**:583–590.

32. Jacquet M, Suortti P. Radiation therapy at compact Compton sources. *Phys Med* 2015;**31**:596–600.

33. Crispi F, Figueras F, Cruz-Lemini M, Bartrons J, Bijnens B, Gratacos E. Cardiovascular programming in children born small for gestational age and relationship with prenatal signs of severity. *Am J Obstet Gynecol* 2012;**207**:121.e1-9.

34. Gonzalez-Tendero A, Torre I, Garcia-Canadilla P, Crispi F, Garcia-Garcia F, Dopazo J, et al. Intrauterine growth restriction is associated with cardiac ultrastructural and gene expression changes related to the energetic metabolism in a rabbit model. *Am J Physiol Hear Circ Physiol* 2013;**305**:H1752-60.

35. Castelli E, Tonutti M, Arfelli F, Longo R, Quaia E, Rigon L, et al. Mammography with synchrotron radiation: first clinical experience with phase-detection technique. *Radiology* 2011;**259**:684–694.

## FIGURES

**1. X-ray phase-contrast synchrotron radiation-based micro-CT imaging of a rat heart. A, B** and **C**, Cardiac anatomy can be observed with great detail: aortic and tricuspid valves (A), fibre orientation (B), false tendon or right ventricle moderator band (C). When doing volume rendering of the images, details of tricuspid (D) or aortic valve (E) can be observed; as well as the atrial pectinate muscles (F and G).

**2. Detail of aortic and ventricular walls of a rat heart.** In the aortic wall layers can be distinguished (A); whereas in the ventricular walls, orientation of fibres can be determined and classified as circumferential (circ) or longitudinal (long) in both right (B) and left (C) ventricles.

**3. Volume rendered images depicting detailed cardiac anatomy of an IUGR and a control heart.** IUGR fetal heart (C) is smaller and with thinner walls compared to the control fetal heart (A). Additionally, it can be appreciated that the coronary vessels are clearly dilated and much more prominent in the IUGR heart (C,D).

**4. Segmentation of the coronary tree.** The coronary tree can be visualized in detail when segmented (A,C). Differences between control (A) and IUGR (C) rabbit fetal hearts are even more evident when the segmentation is visualized as a quantification of lumen diameter (B,D). Lighter colours mean larger diameters; therefore, dilatation of coronary arteries in IUGR (C,D) is clearly visible. In E, the normalized histogram distribution comparing approximated lumen diameter of IUGR versus control (normalized to total amount of vessels) suggests that in IUGR, there is a shift to the right side, i.e. larger diameter, of the histogram, and the relative amount of vessel with smaller diameters (left side) in control heart vessels is higher.

**5. Fibre orientation X-PCI.** Fibre angles change across the walls within a slice in fetal rabbit control (A) and IUGR (B) hearts. Fibre angles change from endo- to epi-cardium from about +60º to -60º. In the C and D, a visualization of the 3D fibre structure of the IUGR rabbit heart is shown (left: fibre angles within one slice; right: 3D fibre tracking within the wall). The histogram of fibre angles for left (E) as well as right ventricle (F) are shown.

**6. Fiber orientation MRI DTI.** Fibre angles change across the walls within a slice in an adult control rabbit (A) and a visualization of the 3D fibre structure within the wall (B). Fibre angles change from endo- to epi-cardium from about +90º to -90º.

**7. Comparison of X-PCI slice and histological section.** (A) Histological section and (B) X-PCI slices perpendicular to the base-apex direction are comparable. Zoom in on the lateral wall of both histological (C) and X-PCI (D) slices demonstrate that fibers are more predominantly circumferential in the mid-myocardium whereas on the endo- and epi-cardium are more longitudinal in both slices.

Supplementary Information

Figure S1: An overview image of the end stage of the measurement setup showing the sample, detector and camera and giving an idea of the distance from the sample to the scintillator.

Figure 1

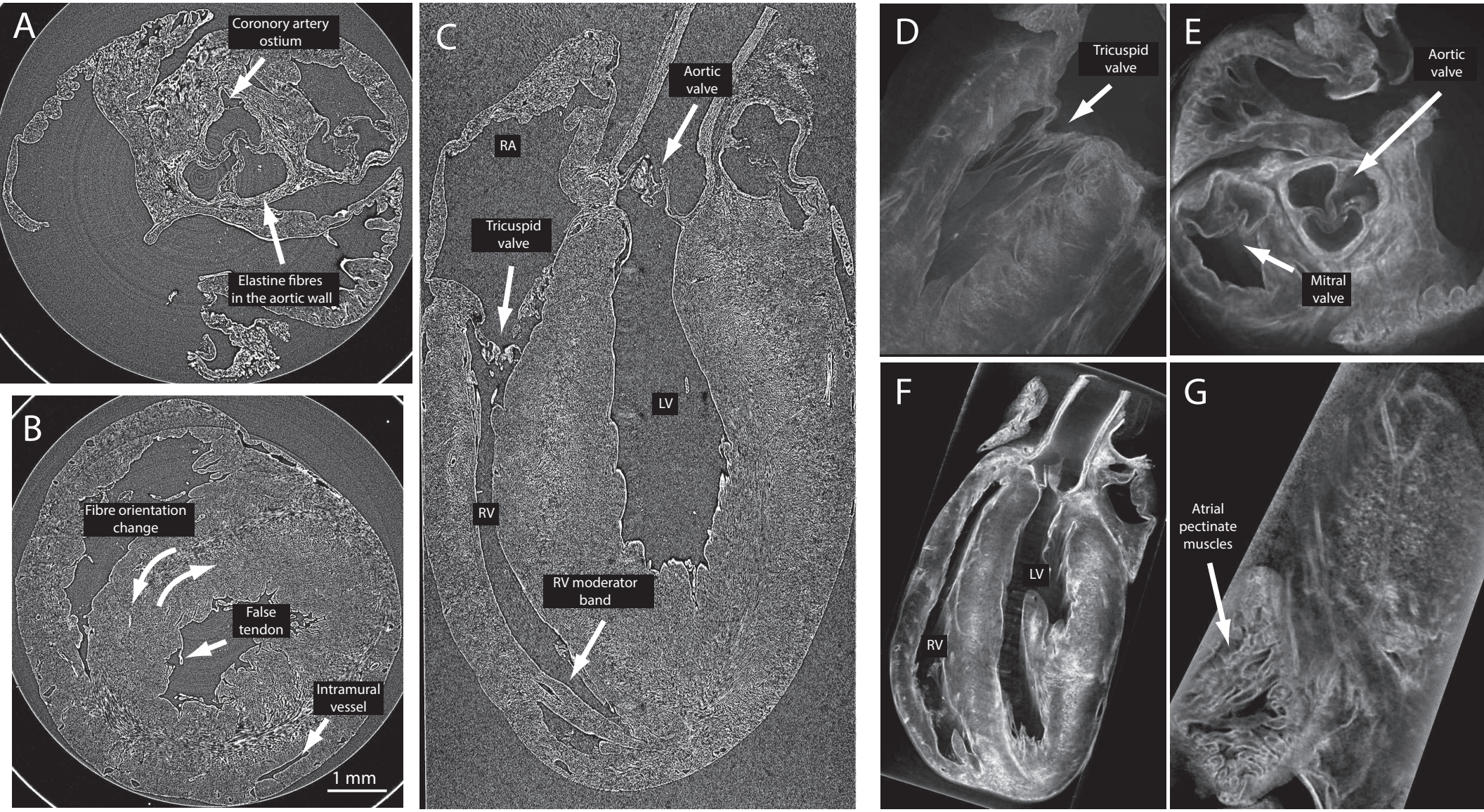
A
Coronory artery ostium
Elastine fibres in the aortic wall
B
Fibre orientation change
False tendon
Intramural vessel
1 mm
C
Aortic valve
RA
Tricuspid valve
LV
RV
RV moderator band
D
Tricuspid valve
E
Aortic valve
Mitral valve
F
LV
RV
G
Atrial pectinate muscles

Figure 2

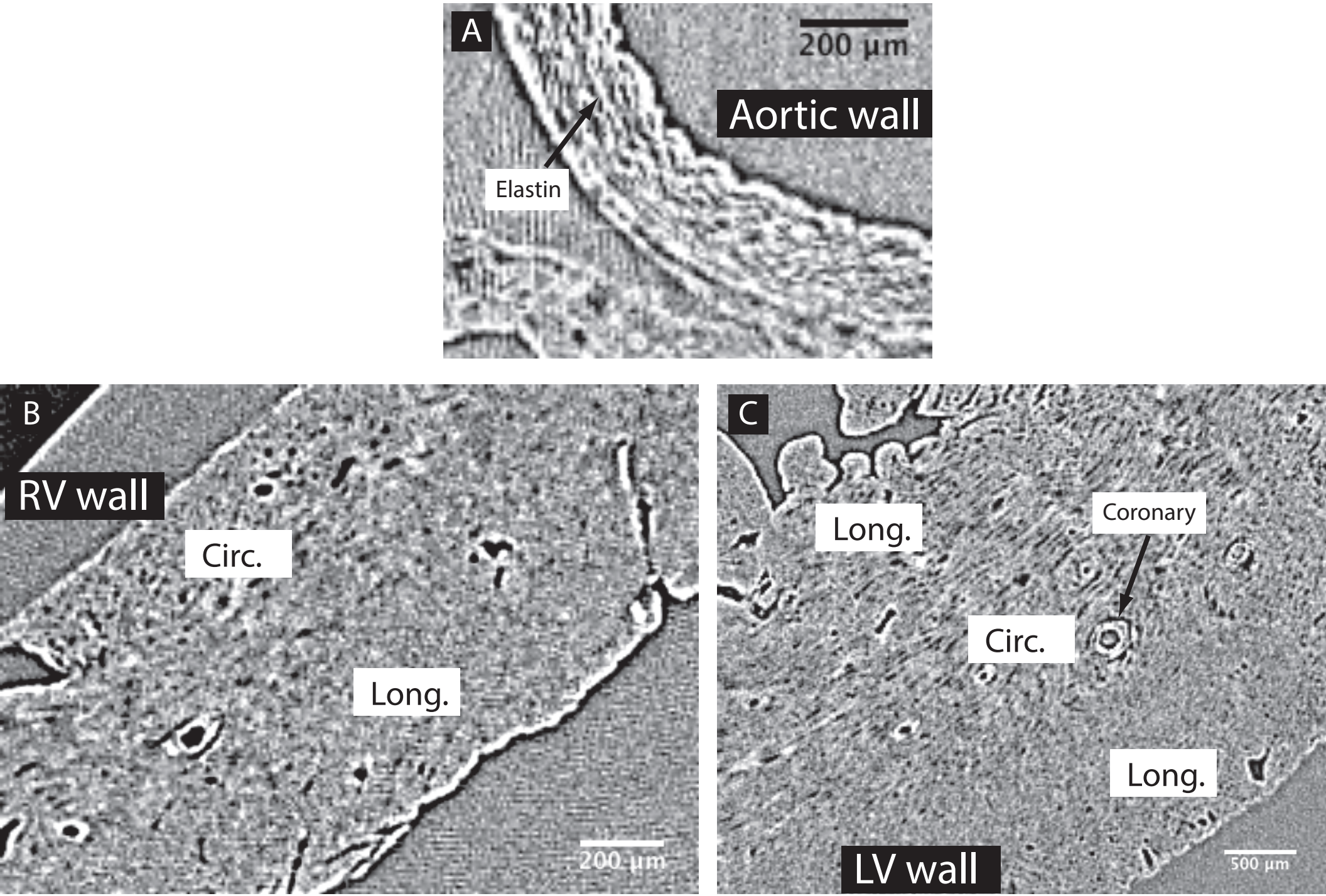
A
200 µm
Aortic wall
Elastin
B
RV wall
Circ.
Long.
200 µm
C
Long.
Coronary
Circ.
Long.
LV wall
500 µm

Figure 3

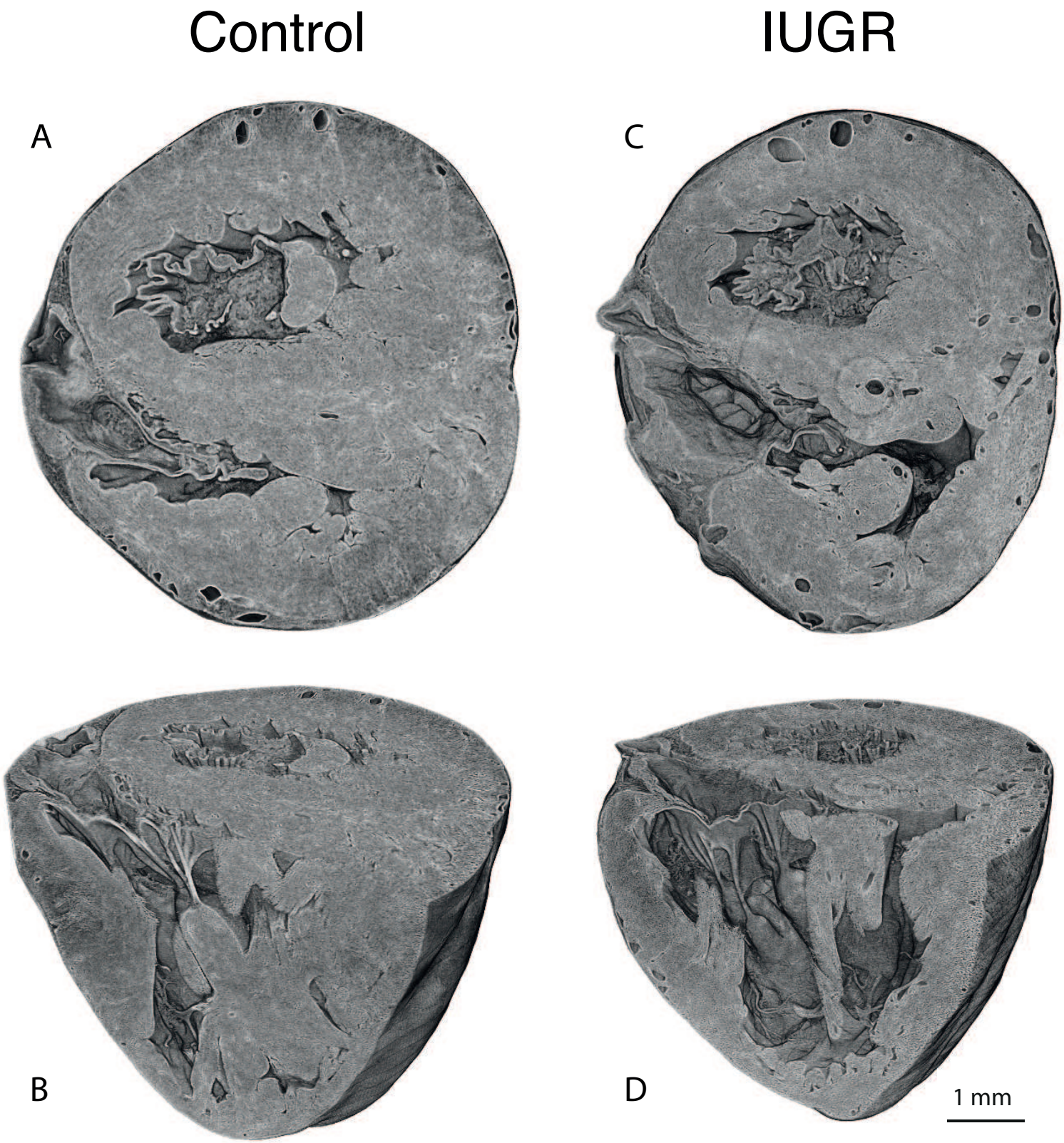

Figure 4

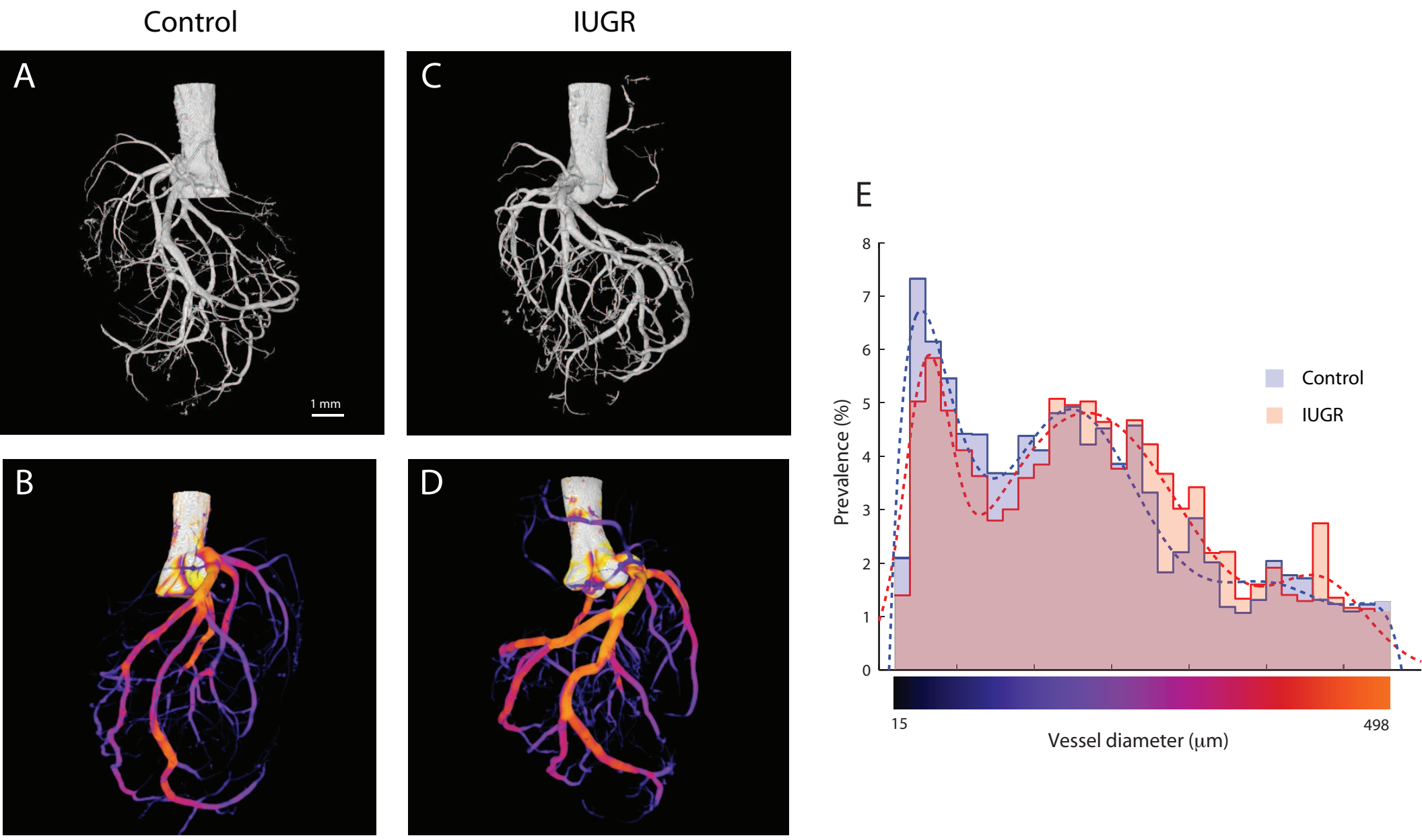
Control
IUGR
A
B
C
D
1 mm
E
Prevalence (%)
0
1
2
3
4
5
6
7
8
Control
IUGR
15
498
Vessel diameter (μm)

Figure 5

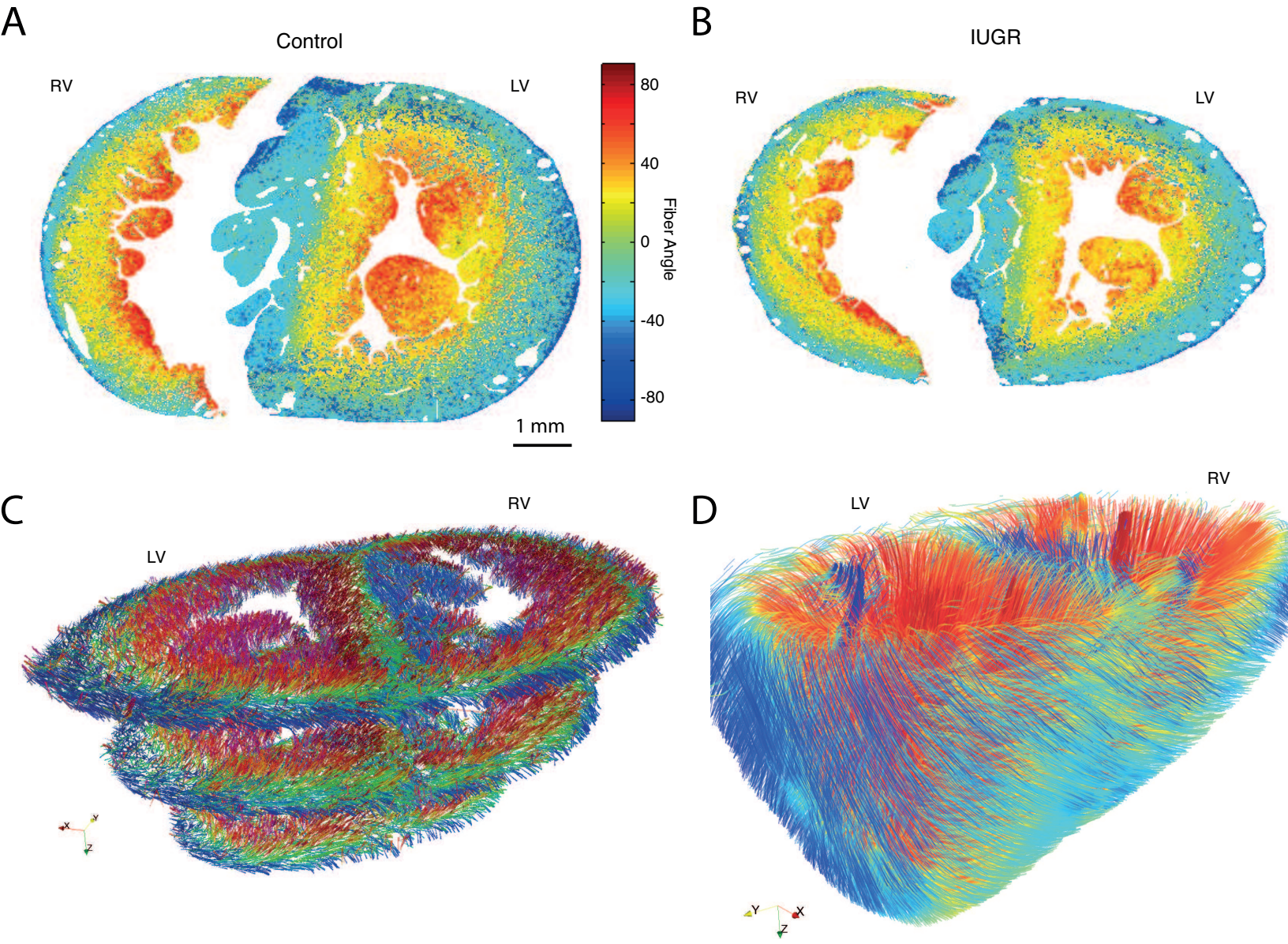
A
Control
RV
LV
80
40
0
-40
-80
Fiber Angle
1 mm
B
IUGR
RV
LV
C
RV
LV
D
LV
RV
E
LV angle histogram
Frequency
0.06
0.05
0.04
0.03
0.02
0.01
0
−80 −60 −40 −20 0 20 40 60 80
Angle (degrees)
F
RV angle histogram
Frequency
0.06
0.05
0.04
0.03
0.02
0.01
0
−80 −60 −40 −20 0 20 40 60 80
Angle (degrees)

Figure 6

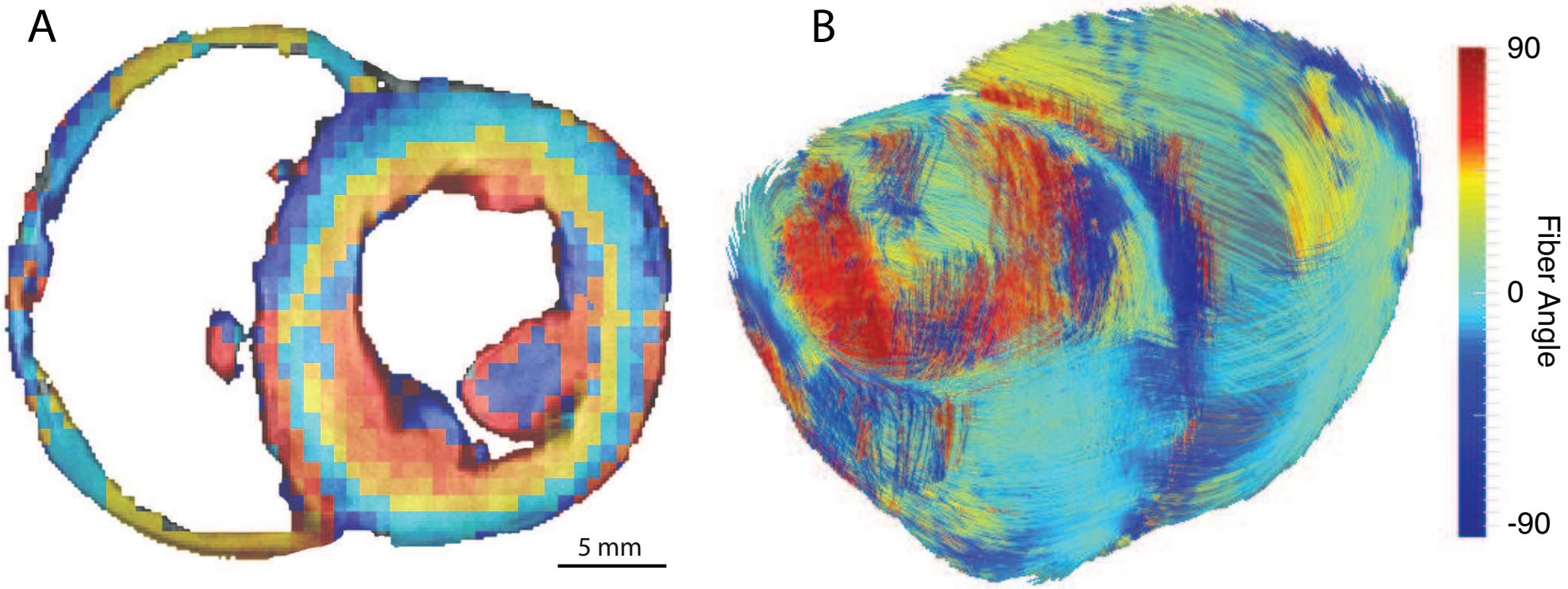

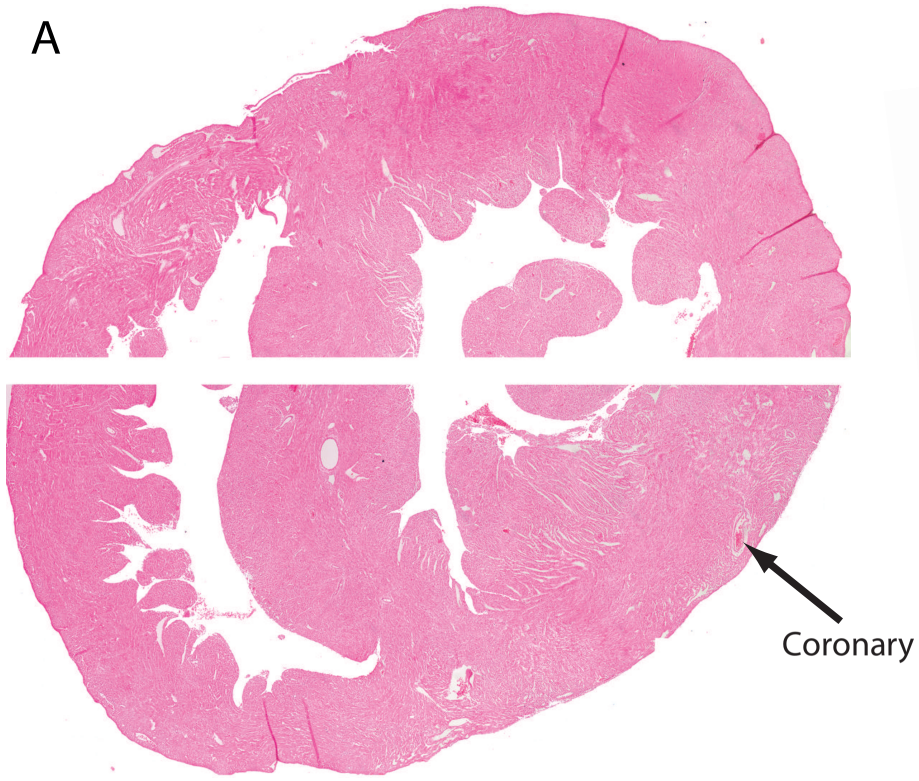
A
Coronary

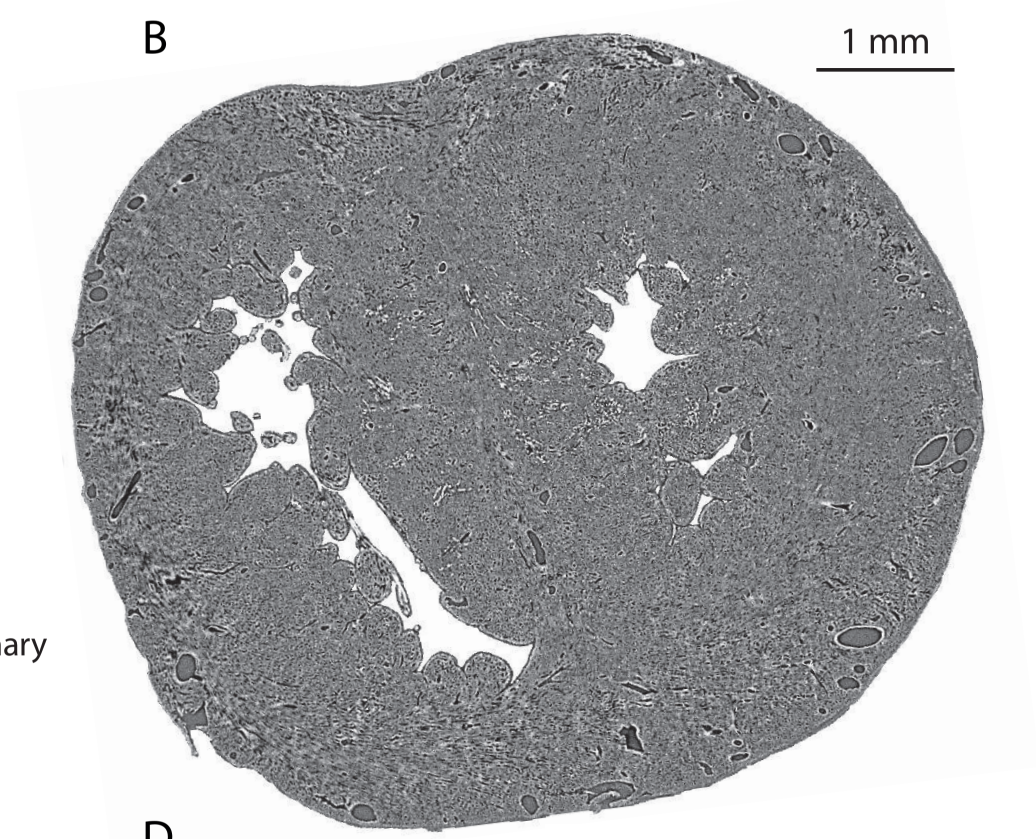
B
1 mm

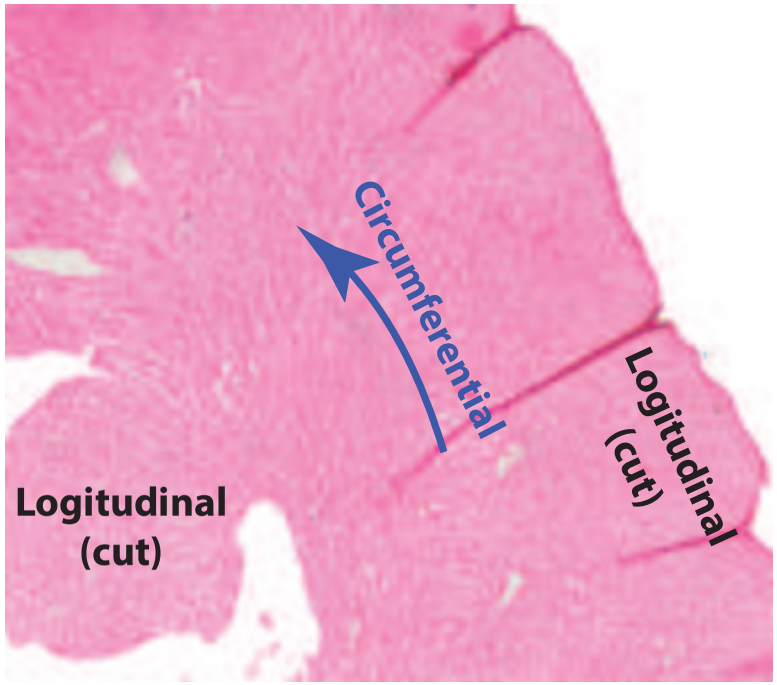
C
Circumferential
Logitudinal
(cut)
Logitudinal
(cut)

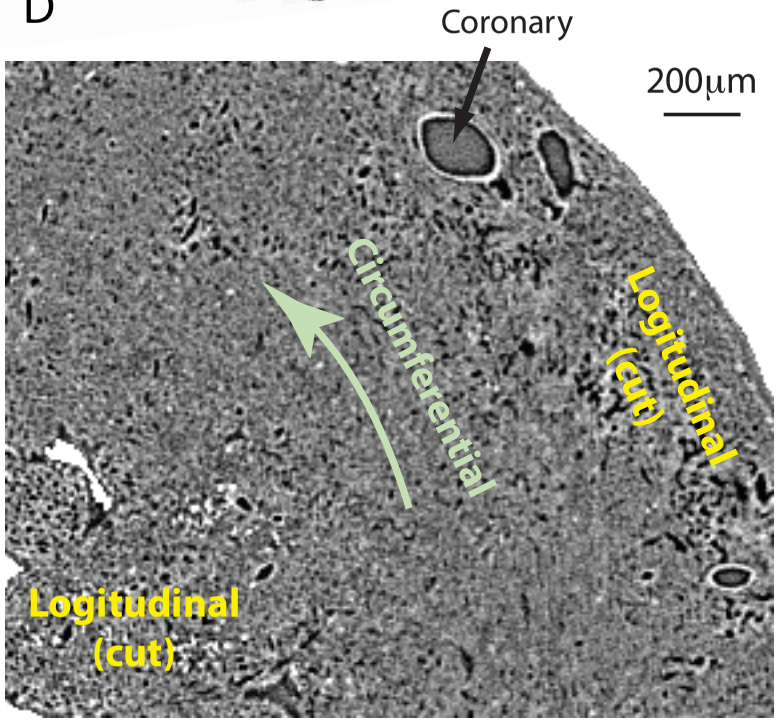
D
Coronary
200μm
Circumferential
Logitudinal
(cut)
Logitudinal
(cut)

Movie 1

Click here to access/download
**Supplemental**
movie1.mov

Movie 2

Click here to access/download
**Supplemental**
movie2.avi

Movie 3

Click here to access/download
**Supplemental**
movie3.mov

Figure S1